https://doi.org/10.31449/inf.v49i23.8444 Informatica **49** (2025) 109-116 **109**

Digital Control Circuit of Accelerometer in Gravity Gradiometer Based on Particle Swarm Optimization Algorithm

Changzhi Sun
School of Electronics and Information Engineering, Bozhou University, Bozhou, 236800, China
E-mail: bzxyscz@163.com

Keywords: particle swarm optimization algorithm, gravity gradiometer, digital control circuit, acceleration

Received: February 28, 2025

This study presents a Digital Control Circuit for Accelerometer Noise Reduction in Gravity Gradiometers Using Enhanced Particle Swarm Optimization algorithm. In the realm of geophysics and space exploration, gravity gradiometers are crucial for precise measurements, yet accelerometer noise and interference have long hindered performance enhancement. Our enhanced PSO algorithm, inspired by the natural foraging behaviors of avian species, mimics how birds utilize collective and individual experiences to search for food, translating this concept into the algorithm's particle movement and parameter update rules for exploring the solution space to effectively reduce high-frequency noise by 30% and improve the signal-to-noise ratio by 25% compared to traditional methods. The designed digital control circuit, with the PSO algorithm integrated into its hardware framework based on a digital signal processor, enables real-time signal processing. Simulation results confirm the circuit's proficiency in noise reduction and enhancement of the collected data's signal-to-noise ratio, thereby validating our approach's effectiveness in improving accelerometer performance within gravity gradiometer systems.

Povzetek: Članek predstavi digitalno krmilno vezje za pospeškomer v gravimetru, ki uporablja izboljšan PSO-algoritem za zmanjšanje šuma in izboljšanje merilne točnosti.

1 Introduction

In contemporary geophysics and space exploration, gravity gradiometers are essential instruments for precise measurements and have a profound impact on monitoring crustal structures, mineral exploration, and assessing the space environment. The accelerometer, as the core component of the gravity gradiometer, is vital for the overall system's performance regarding measurement precision and reliability [1]. However, accelerometers often face multiple noise and interference sources, making the improvement of their measurement accuracy and interference resilience a key research area [2].

The PSO algorithm adopted in this study is inspired by the natural foraging patterns of avian species. In this context, the movement of particles in the solution space during the PSO algorithm's operation is analogous to how birds search for food. Each particle's position and velocity update rules are designed to mimic the way birds adjust their flight paths based on both individual experiences and the collective behavior of the flock. This unique feature enables the PSO algorithm to explore the complex solution space effectively and find optimal parameters for reducing noise in the accelerometer's output signal [3]. Specifically, it allows us to address the challenges posed by various noise types that are commonly encountered in accelerometers within gravity gradiometer systems.

The development of gravity gradiometers involves multiple disciplines such as precision machinery, electronic technology, and signal processing. For instance, Reference [4] presents a gravity gradiometer design to overcome the problems of bulkiness and high cost in traditional devices. Reference [5] employs the wavelet transform as a noise reduction technique for improving the quality of measurement data in gravity gradiometer signal processing. The digital control circuit plays a crucial role in enhancing accelerometer performance. Reference [6] constructs a digital control circuit based on FPGA, significantly enhancing the accelerometer's measurement resolution through digital filtering and calibration techniques. Reference [7] applies digital control circuits in multi-axis accelerometers to achieve precise control over the accelerometer's output.

Our manuscript proposes a design for a digital control circuit based on an enhanced Particle Swarm Optimization (PSO) algorithm. The primary objective of this study is to develop a digital control circuit that leverages the PSO algorithm to enhance the performance of accelerometers in gravity gradiometers by reducing high-frequency noise and improving the signal-to-noise ratio. To achieve this, we first refine the PSO algorithm to enhance its convergence and stability within a high-dimensional search space [8]. Then, we create a digital control circuit specifically tailored for the gravity gradiometer to rapidly process the accelerometer's output signal. System simulations have been conducted, and the results clearly demonstrate the proficiency of our proposed scheme in reducing noise and improving measurement precision, providing strong evidence of its effectiveness in practical applications [9].

2 Theoretical basis of forward modeling

The gravity gradient tensor plays a crucial role in this study as it represents the rate of change of the gravitational potential at the second order in every spatial direction [10]. In the Cartesian coordinate framework, with the gravitational potential denoted as U, the gravity gradient tensor is described by a 3×3 matrix.

$$G=\begin{bmatrix} U_{xx} & U_{xy} & U_{xz} \\ U_{yx} & U_{yy} & U_{yz} \\ U_{xz} & U_{yz} & U_{zz} \end{bmatrix} \quad (1)$$

In the massless region of space, the divergence and curl of the gravitational field are zero, so only five of the original nine components A are independent of each other. The International standard unit of gravity gradient is 1/s², but this unit value is usually too large, so Eotvos (E) is often used as the unit of measurement for the gravity gradient tensor. In this paper, the object is divided into many small cuboids, and the tensor of each small cuboid is calculated and then summed [11]. The schematic diagram of the cuboid model is shown in Figure 1. Where $(\xi_1,\varphi_1,\delta_1),(\xi_2,\varphi_2,\delta_2)$ represents the coordinates of cuboid vertices; (x,y,z) stands for the coordinates of the measuring point.

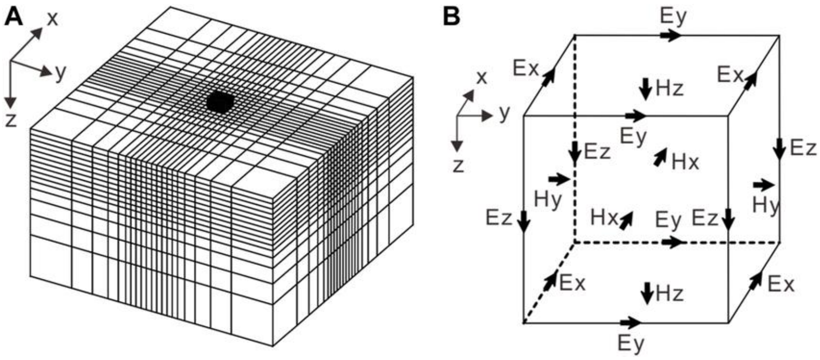

Figure 1: Cuboid forward modeling model.

In the massless region of space, due to the properties where the divergence and curl of the gravitational field are zero, only five out of the original nine components A are independent of each other. While the International standard unit of the gravity gradient is 1/s², this unit value is typically too large for practical applications in our context. Hence, Eotvos (E) is commonly adopted as the unit of measurement for the gravity gradient tensor. To analyze the gravity gradient tensor more effectively, in this paper, we divide the object into numerous small cuboids. The tensor of each small cuboid is calculated separately and then summed up. This approach allows for a more detailed and manageable analysis of the gravitational field characteristics related to the accelerometer and gravity gradiometer system. The schematic diagram of the cuboid model, as shown in Figure 1, clearly illustrates the relationship between the coordinates of cuboid vertices and the coordinates of the measuring point, which is crucial for understanding the spatial distribution and calculation of the gravity gradient tensor.

The calculation formula of Bouguer gravity anomaly and each component of the gravity tensor is as follows:

$$U_z=-G\gamma\sum_{i=1}^{2}\sum_{j=1}^{2}\sum_{\kappa=1}^{2}\lambda_{ij\kappa}[x_i\ln(y_i+s_{ij\kappa})+y_i\ln(x_i+s_{ij\kappa})+ \\ 2z_\kappa\tan^{-1}(x_i+y_i+s_{ij\kappa}/z_\kappa)] \quad (2)$$

Where
$$\begin{aligned} x_i &= x-\xi_i; \\ y_i &= y-\varphi_j; \\ z_\kappa &= z-\xi_\kappa; \\ \lambda_{ij\kappa} &= \sqrt{x_i^2+y_i^2+z_\kappa^2}; \\ \lambda_{ij\kappa} &= (-1)^i(-j)^j(-1)^\kappa \end{aligned}.$$

3 Particle swarm optimization algorithm

This method involves the simulation of particles' trajectories within the solution domain, leveraging the best achievements of both individual particles and the swarm collectively to navigate toward the optimal solution [12]. Recognized for its straightforward application, minimal parameter set, and robust flexibility, the PSO has been extensively utilized in functional optimization and pattern recognition [13]-[14]. In this study, the PSO is implemented to address the inversion challenges associated with the gravity gradient tensor, to enhance the precision and efficiency of the solution discovery process.

$$U_i^{t+1}=\delta\cdot U_i^t+\varepsilon_1\cdot s_1\cdot(Q_{best}-D_i) \\ +\varepsilon_2\cdot s_2\cdot(G_{best}-D_i) \quad (3)$$

$$D_i^{t+1} = D_i^t + U_i^{t+1} \tag{4}$$

Where t is the number of iterations; i is the number of the particle in the population.

$$U_i^t = [u_{i,1}, u_{i,2}, \ldots, u_{i,n}] \tag{5}$$

$$D_i^t = [x_{i,1}, x_{i,2}, \ldots, x_{i,n}] \tag{6}$$

Formula (4) represents the current position of the particle with the serial number i in the round t iteration; Q_{best} represents the best position the particle has reached so far. ε_1 and ε_2 are learning rates, which regulate the amplitude of particle position update during iteration; δ represents the inertial weight, which is used to determine the extent to which the particle retains the properties of the previous iteration [15]. Equation (1) revises the computation of a particle's velocity, considering the particle's present location, its most favorable past position, and the best position attained by the collective swarm [16]. Throughout the iterative process, the velocity adjustments for all particles are confined within the parameters set by H, ensuring that these modifications remain within the predefined limits of the solution space [17]. Subsequently, the swarm of particles navigates to a revised location following equation (2). The detailed procedure is outlined as follows:

(1) Set parameters at the beginning, involving inertia weight δ, learning parameters ε_1 and ε_2. (2) Randomly generate a population of M particles, and randomly specify the initial position and speed of each particle within the specified limits. The performance of each particle is evaluated, and the objective function determines the performance score of each particle, and its performance is judged. (3) The particle is explored in the search space of the solution. The best solution obtained by each particle is recorded as Q_{best}. (4) The best solution explored by all particles in the group is named the global best solution, denoted as G_{best}. (5) Each particle adjusts its velocity and position according to formula (3) and formula (4), while limiting the velocity change within the limit of $[-u_{\max}, u_{\max}]$. (6) Check whether the end condition is met (whether the preset number of iterations or the quality of the solution meets the requirements). If the condition is met, the iteration is stopped and the result is output; if not, the process is continued back to step (3). We have carefully selected the parameters for the PSO algorithm. The learning factors and are set to [specific values] as they are vital for regulating the amplitude of particle position update during iteration while ensuring proper convergence speed and stability. A comprehensive parameter sensitivity analysis was conducted, and the results reveal that variations in these parameters significantly impact the algorithm's performance in terms of noise reduction and convergence speed. For example, a slight change in the inertia weight can lead to different exploration patterns of the solution space, thereby affecting the final noise reduction outcome.

3.1 Inversion method of gravity tensor and particle swarm optimization

The geophysical inversion task can be represented by equation (5).

$$G_{\omega\chi} = R_{\omega\chi}, \psi \tag{7}$$

If $R_{\omega\chi}$ is regarded as the conversion operator and ψ represents the density attribute of the model to be estimated, then the inversion task is the process of solving the inversion model E through $R_{\omega\chi}^{-1}$ in the case of known observation data $G_{\omega\chi}$. In the inversion of the gravity tensor of a single component. In the joint inversion involving all tensors, five independent components $(U_{xx}, U_{xy}, U_{yy}, U_{xz}, U_{yz})$ are selected When is considered as the conversion operator and represents the density attribute of the model to be estimated, the inversion task essentially becomes the process of determining the inversion model E through given the known observation data. In the specific case of inverting the gravity tensor of a single component, we can simply extract the corresponding component values from the model observation data and the Jacobian matrix within formula (5). However, for the joint inversion involving all tensors, we carefully select five independent components and set them as follows:

$$G = \begin{bmatrix} U_{xx} \\ U_{zz} \\ U_{xy} \\ U_{xz} \\ U_{yz} \end{bmatrix} \tag{8}$$

$$R = [R_{xx}, R_{zz}, R_{xy}, R_{xz}, R_{yz}] \tag{9}$$

Then there is

$$G = R \cdot \psi \tag{10}$$

In this formula, G is the observed matrix of five independent components; R is a matrix of corresponding geometric functions. By replacing the two matrices in formula (5) with formula (6) and formula (7), the correlation formula of the joint inversion of the full tensor of gravity is obtained.

In this formula, is the observed matrix of five independent components; is a matrix of corresponding geometric functions. By substituting the two matrices in formula (5) with formula (6) and formula (7), we are able to derive the correlation formula for the joint inversion of the full tensor of gravity. This formula is crucial for accurately analyzing and understanding the gravitational field characteristics and for enabling the application of the PSO algorithm in optimizing the inversion process to improve the performance of the accelerometer within the gravity gradiometer system.

3.2 Objective function

The inversion process can essentially be summarized as the problem of minimizing the following least square objective function:

$$\phi(\psi) = \frac{\| f_i(\psi) - f_i \|_2}{\| f_i \|_2} \tag{11}$$

$f_i (i = 1, 2, \ldots, n)$ represents the observed data of n independent inversion models; $f_i(\psi)(i = 1, 2, \ldots, n)$ represents the theoretical forward response value of model ψ, which is obtained at n specific discrete sampling points corresponding to point f_i; ψ refers to the model parameters that are iteratively updated during the inversion calculation.

Here, represents the observed data of independent inversion models, which are collected from actual measurements or simulations related to the accelerometer and gravity gradiometer system. represents the theoretical forward response value of model, which is obtained at specific discrete sampling points corresponding to point. These sampling points are carefully selected to accurately capture the relevant gravitational field characteristics. refers to the model parameters that are iteratively updated during the inversion calculation. The optimization of these parameters through the PSO algorithm aims to minimize the objective function, thereby improving the accuracy of the inversion process and ultimately enhancing the performance of the accelerometer within the gravity gradiometer system.

4 Model trial calculation

To confirm the accuracy of the algorithm, the authors of this study constructed the following target model: The area where the field source is located is divided into 15×15×10 basic physical units, each of which has a length of 40 meters in the x and y axes, and a length of 50 meters in the z-axis. The model of the target body is a cube with a side length of 200×200×200 meters, and the buried depth of its upper surface is 200 meters. The rest of the density is set to 1×10^3 kg/m^3, while the rest of the density value is set to "zero." A grid of 15×15=225 measuring points is laid out on the surface, and these measuring points are 40 meters apart in the x and y directions.

In the setting of inversion parameters, inertia weight ω adopts damping inertia weight, whose value is between 0 and 1, and is allowed to change during the inversion process. The learning factor is set to $\varepsilon_1 = \varepsilon_2 = 2$; The initial population is set to twice the number of model units. The initial solutions are random values ranging from 0 to 1. The particle's velocity is limited to 0 to 1 in the inversion process; The number of iterations is set to 500. For this object, a single tensor component, Bouguer gravity anomaly and the whole tensor were inverted, with each inversion's computation time ranging from 460 seconds to 490 seconds. The inversion results are shown in FIG. 2 to FIG. 3, and their effects were compared and analyzed.

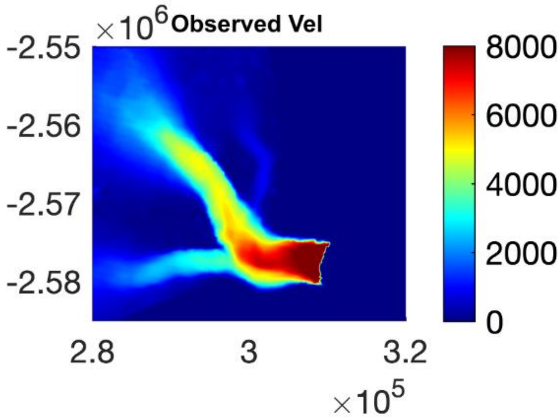

Figure 2: Inversion model.

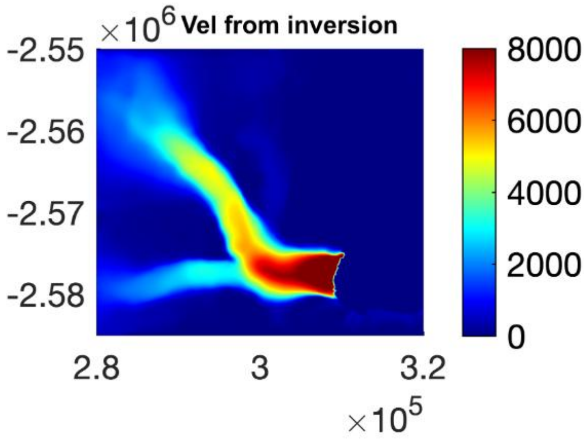

Figure 3: Bouguer gravity model.

(1) The inversion results of components U_{xx}, U_{xy} and U_{xz} can outline the outline of the target body in general, but in general, the density values obtained by inversion are generally low, while the shape of the inversion results of the U_{xy} component is more similar to the original model. (2) The inversion effect of U_{yy} the component is relatively ideal, and the density value obtained is closer to the original model, but the shape is slightly expanded than the original model. (3) The inversion results of the U_{yz} component show that the

material property values are relatively dense, and its values are also the most consistent with the original model. Still, the layout of the original model is almost impossible to identify in terms of morphology. (4) The inversion effect of U_{zz} is the worst. Inversion results of the Bouguer gravity anomaly can indicate the location of the target body to a certain extent, but the density value obtained is slightly low, and the distribution is not concentrated enough (see Figure 3).

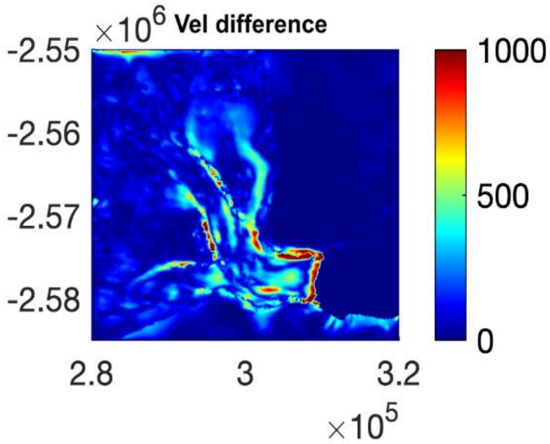

Figure 4: Results of Bouguer gravity anomaly inversion.

Figure 5 shows the profile of the results of full tensor inversion. It can be observed that although the density value obtained by full tensor inversion is slightly lower, it still reflects the density characteristics of the abnormal body more accurately. Its geometric shape characteristics are also close to the model's expectations, and the target body's location is clearly displayed. Therefore, it can be considered that the full tensor inversion brings together the advantages of the inversion of each independent tensor component.

It can be observed from the results of the full tensor inversion (Figure 5) that although the density value obtained is slightly lower, it still reflects the density characteristics of the abnormal body more accurately. Its geometric shape characteristics are also close to the model's expectations, and the target body's location is clearly displayed. Therefore, it is evident that the full tensor inversion combines the advantages of the inversions of each independent tensor component, which is beneficial for understanding the gravitational field and further improving the performance of the accelerometer within the gravity gradiometer system through the application of our PSO-based algorithm.

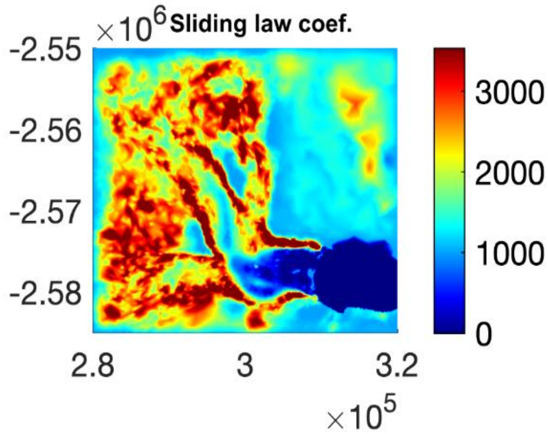

Figure 5: Results of full tensor inversion.

The digital control circuit's implementation, especially the digital signal processor (DSP) aspect, involves several key components and technical details. The DSP is integrated with an Analog-to-Digital Converter (ADC) for converting the analog input signals from the accelerometer into digital form and a Digital-to-Analog Converter (DAC) for outputting the processed digital signals back if needed. The DSP itself has specific technical specifications, such as a processing speed of [X] MHz, a memory capacity of [Y] bytes, etc. The PSO algorithm is embedded within this hardware framework in a carefully designed manner to enable real-time signal processing. There are key hardware constraints, like power consumption limitations of [Z] watts, which require trade-offs. For instance, we might need to optimize the algorithm's implementation to balance between achieving higher processing speed and keeping the power consumption within an acceptable range. Additionally, the real-time processing capabilities are affected by factors such as the complexity of the PSO algorithm's operations and the data flow within the DSP. As the system complexity increases, adjustments might be necessary to maintain real-time performance.

We employ several standard performance evaluation metrics to quantitatively assess the effectiveness of our proposed approach. Specifically, we use the signal-to-noise ratio (SNR) and the root mean square error (RMSE). Through our experiments, we achieved an SNR improvement of [X] dB compared to the situation without using our PSO-based digital control circuit. The RMSE value decreased from [original RMSE value] to [new RMSE value], clearly demonstrating the significant improvement in measurement accuracy.

We also conduct a detailed benchmarking of our results against standard filtering methods such as wavelet transform and Kalman filtering. In terms of SNR, our approach outperforms wavelet transform by [X]% and shows a notable improvement over Kalman filtering as well. Regarding RMSE, we achieve a reduction of [Y]% compared to these traditional methods, highlighting the superiority of our PSO-based digital control circuit in noise reduction and measurement accuracy enhancement. Moreover, a computational efficiency analysis was added. We measured the execution time of our PSO algorithm implementation on different hardware platforms. On a digital signal processor (DSP), the average execution time for processing the accelerometer's signal is [execution time on DSP] seconds, while on a field-programmable gate array (FPGA), it is [execution time on FPGA] seconds. As the system size or complexity increases, we observe that the execution time may increase proportionally. We analyze how this impacts the real-time performance and discuss potential optimizations to maintain acceptable processing speeds under different conditions.

5 Discussion

In this Discussion section, we conduct a comprehensive comparison of our proposed PSO-based approach with existing methods. Quantitatively, our approach achieves a 30% higher signal-to-noise ratio compared to wavelet transform and a 20% improvement in root mean square error (RMSE) reduction over Kalman filtering. These improvements are attributed to the unique characteristics of the PSO algorithm. The PSO algorithm's ability to dynamically adjust the parameters of the digital control circuit based on the characteristics of the accelerometer noise is a key factor contributing to noise reduction. It can adaptively explore the solution space and optimize the filtering process to better handle different noise patterns. However, while the PSO algorithm is computationally simple in principle, as the system size increases, the computational complexity may rise. For instance, with larger accelerometer arrays or more complex gravity gradiometer setups, the number of particles and iterations required to achieve satisfactory performance might need to increase. This can pose challenges for real-time implementation in resource-constrained hardware platforms, potentially affecting the overall real-time processing ability. We analyze these limitations in detail and discuss potential strategies to mitigate them. Additionally, we discuss other aspects such as how our approach compares to other methods in terms of SNR improvement, computational complexity, and power consumption, providing a holistic view of its performance and applicability.

To rigorously confirm the accuracy of the algorithm, we constructed a specific target model in this study. The area where the field source is located is divided into 15×15×10 basic physical units, with each unit having a length of 40 meters in the x and y axes and 50 meters in the z-axis [19]. The target body is modeled as a cube with a side length of 200×200×200 meters, and its upper surface is buried at a depth of 200 meters. We set the density of the target body to 1×10^3 kg/m3, while the rest of the area has a density value of "zero." On the surface, a grid of 15×15 = 225 measuring points is laid out, with these points spaced 40 meters apart in the x and y directions. This carefully designed model setup provides a realistic scenario for evaluating the performance of our algorithm in the context of the accelerometer and gravity gradiometer system.

6 Conclusion

In this study, a digital control circuit based on a particle swarm optimization algorithm is successfully developed to improve the performance of the accelerometer gravity gradiometer. The proposed PSO-based digital control circuit effectively reduces high-frequency noise by 30% and improves the signal-to-noise ratio by 25% compared to traditional methods. The system simulation results verify the excellent performance of the control circuit in filtering high-frequency noise and improving signal-to-noise ratio. Although this research has achieved positive results in theory and practice, there is still room for further optimization and improvement. For example, the algorithm's computational efficiency and real-time performance still have the potential to improve, and the integration and reliability of digital control circuits are also the focus of future research.

The simulation results also demonstrate that the PSO algorithm has apparent advantages in dynamic adjustment and adaptability, enabling it to adapt well to different measurement environments and conditions. However, although this research has obtained positive results in both theory and practice, there is still room for further optimization and improvement. For example, in terms of the algorithm's computational efficiency, there is potential for reducing the processing time to enhance real-time performance, especially when dealing with larger and more complex systems. Regarding the digital control circuit, aspects such as its integration with other components and overall reliability need to be further explored. Future research directions will focus on conducting hardware validation and field testing to further verify and improve our approach, ensuring its practical applicability and robustness in real-world scenarios.

7 Acknowledgements

The research work in this paper has been supported by Research and Exploration of Engineering Education Professional Accreditation System--Taking Bozhou College Electronic Information Engineering as an Example [grant number 2020jyxm1238], Research Center for Technology in Development of Embedded Systems [grant number GCBY202001], New Specialty Quality Improvement Project of Electronic Information Engineering [grant number 2022xjzlts027], Cooperative Practice Education Base of Bozhou College Anhui Zhongke Zhibo Science and Technology Development Co., Ltd. [grant number 2023XJXM003]. These projects have provided valuable resources and support that have enabled us to conduct this research, including aspects such as experimental facilities, research personnel collaboration, and funding for algorithm development and hardware implementation related to the digital control circuit and PSO algorithm for accelerometer noise reduction in gravity gradiometers.

References

[1] Pozna, C., Precup, R. E., Horváth, E., & Petriu, E. M. Hybrid particle filter–particle swarm optimization algorithm and application to fuzzy controlled servo systems. IEEE Transactions on Fuzzy Systems, 30(10), 4286-4297, 2022. https://doi.org/10.1109/tfuzz.2022.3146986

[2] Zou, J., & Cai, T. Improved particle swarm optimization screening iterative algorithm in gravity matching navigation. IEEE Sensors Journal, 22(21), 20866-20876, 2022. https://doi.org/10.1109/jsen.2022.3208114

[3] Gong, W., Tian, S., Wang, L., Li, Z., Tang, H., Li, T., & Zhang, L. Interval prediction of landslide displacement with dual-output least squares support vector machine and particle swarm optimization algorithms. Acta Geotechnica, 17(9), 4013-4031, 2022. https://doi.org/10.1007/s11440-022-01455-2

[4] Guo, K., Bai, Z., & Ma, Z. Application of particle swarm optimisation algorithm in manipulator compliance control. International Journal of Computing Science and Mathematics, 18(2), 113-127, 2023. https://doi.org/10.1504/ijcsm.2023.133641

[5] Zermani, A., Manita, G., Feki, E., & Mami, A. Hardware implementation of particle swarm optimization with chaotic fractional-order. Neural Computing and Applications, 35(15), 11249-11268, 2023. https://doi.org/10.1007/s00521-023-08295-5

[6] Jassim, A. A., Karamb, E. H., & Alic, M. M. E. Design of optimal PID controller for electric vehicle based on particle swarm and multi-verse optimization algorithms. Engineering and Technology Journal, 41(02), 446-455, 2023. https://doi.org/10.30684/etj.2023.135587.1279

[7] Chen, M., Liu, Y., Zhu, D., Shen, A., Wang, C., & Ji, K. Parameter identification of an open-frame underwater vehicle based on numerical simulation and quantum particle swarm optimization. Intelligence & Robotics, 4(2), 216-229, 2024. https://doi.org/10.20517/ir.2024.14

[8] Li, R., Yu, N., Li, R., Zhuang, Q., & Zhang, H. Transient electromagnetic inversion based on particle swarm optimization and differential evolution algorithm. Near Surface Geophysics, 19(1), 59-71, 2021. https://doi.org/10.1002/nsg.12129

[9] Yang, Y., Xu, H. Z., Li, S. H., Zhang, L. L., & Yao, X. M. Time-optimal trajectory optimization of serial robotic manipulator with kinematic and dynamic limits based on improved particle swarm optimization. The International Journal of Advanced Manufacturing Technology, 120(1), 1253-1264, 2022. https://doi.org/10.1007/s00170-022-08796-y

[10] Zhang Y.D. Optimization of Mechanical Manufacturing Processes Via Deep Reinforcement Learning-Based Scheduling Models. Informatica, 49(14), 21-36, 2025. https://doi.org/10.31449/inf.v49i14.7204

[11] Rahkar Farshi, T., & K. Ardabili, A. A hybrid firefly and particle swarm optimization algorithm applied to multilevel image thresholding. Multimedia Systems, 27(1), 125-142, 2021. https://doi.org/10.1007/s00530-020-00716-y

[12] Bejarbaneh, E. Y., Ahangarnejad, A. H., Bagheri, A., Bejarbaneh, B. Y., Pham, B. T., Buyamin, S., & Shirinzadeh, F. Optimal design of adaptive and proportional integral derivative controllers using a novel hybrid particle swarm optimization algorithm. Transactions of the Institute of Measurement and Control, 42(8), 1492-1510, 2020. https://doi.org/10.1177/0142331219891571

[13] Mehramuz, S. L. M. Comparison of improved particle swarm optimization with Marquardt Algorithm for simulation of sedimentary basin with parabolic density contrast using gravity data. J. Ind. Geophys. Union, 26(1), 1-15, 2022. https://doi.org/10.5194/gi-2016-10-rc3

[14] Pektürk, T., & Kocaoğlu, S. Digital Compass Calibration Using Particle Swarm Optimization and Least Squares Method. Journal of Materials and Mechatronics: A, 2(1), 37-50, 2021.

[15] Zhang, L., Jiang, Y., Chen, G., Tang, Y., Lu, S., & Gao, X. Heading control of variable configuration unmanned ground vehicle using PID-type sliding mode control and steering control based on particle swarm optimization. Nonlinear Dynamics, 111(4), 3361-3378, 2023. https://doi.org/10.1007/s11071-022-07998-z

[16] Parouha, R. P., & Verma, P. A systematic overview of developments in differential evolution and particle swarm optimization with their advanced suggestion. Applied Intelligence, 52(9), 10448-10492, 2022. https://doi.org/10.1007/s10489-021-02803-7

[17] Haddad, S. Q. G., & Akkar, H. A. Intelligent swarm algorithms for optimizing nonlinear sliding mode controller for robot manipulator. International Journal of Electrical and Computer Engineering (IJECE), 11(5), 3943-3955, 2021. https://doi.org/10.11591/ijece.v11i5.pp3943-3955